

Article

Quaternary Evolutionary Stages of Selinitza Cave (SW Peloponnese, Greece) Reveal Sea-Level Changes Based on 3D Scanning, Geomorphological, Biological, and Sedimentological Indicators

Isidoros Kampolis ¹, Stavros Triantafyllidis ^{1,*}, Vasilios Skliros ¹ and Evangelos Kamperis ²

¹ School of Mining and Metallurgical Engineering, National Technical University of Athens, 15773 Athens, Greece; kampolisgeo@gmail.com (I.K.); sklirosbill@gmail.com (V.S.)

² Independent Researcher, 11147 Athens, Greece; ekamperis@hotmail.gr

* Correspondence: striantafyllidis@metal.ntua.gr; Tel.: +30-2107724468

Abstract: Significant evolutionary stages of Selinitza Cave (SW Peloponnese, Greece) were revealed by 3D mapping, as well as geomorphological study of the cave and the nearby landscape. Four marine terraces were identified in the area of the coastal cave at 6, 10.7, 16.6, and 30–32 m above sea level (asl), with the terrace at 16.6 m representing Marine Isotope Stage (MIS) 5. The widest karstified space of Selinitza Cave clusters between 15.73 and 18.05 m above sea level (asl), with the peak lying at 16.4 m asl, corresponding to the level where the phreatic/epiphreatic zone was stable for a sufficient period of time. A tidal notch at 16.4 m asl at the cave entrance is correlated to the marine terrace at 16.6 m. Both features correspond to the sea-level stand at which intense karstification occurred. The tidal notch bears a horizontal arrangement of *Lithophaga* borings at the vertex. Sedimentological investigation of the Selinitza fine-grained deposit revealed the paleohydrologic regime of the cave. It is characterized by “slack-water” facies, indicating very low water flow speeds, whereas the thickness of the deposit points to stable hydrological conditions for prolonged periods. The cave sediment height of 18.8 m asl indicates a flooding level higher than sea level. The overlying Plattenkalk flysch is most probably the major source of detritus, and the predominance of authigenic dolomite (>98% modal in the carbonate fraction) indicates a hyposaline environment related to mixing of sea water with percolating fresh water. The approach of this study shows the significance of 3D mapping, bio-geo-Relative Sea Level (RSL) indicators, and sedimentology in deciphering the paleogeographic evolution of coastal karstic systems and subsequently defining the paleoclimate regime of coastal areas in Greece and the eastern Mediterranean during the Late Quaternary.

Keywords: 3D mapping; tidal notches; *Lithophaga* borings; marine terraces; authigenic dolomite; slack-water facies; Late Quaternary



Citation: Kampolis, I.; Triantafyllidis, S.; Skliros, V.; Kamperis, E.

Quaternary Evolutionary Stages of Selinitza Cave (SW Peloponnese, Greece) Reveal Sea-Level Changes Based on 3D Scanning, Geomorphological, Biological, and Sedimentological Indicators.

Quaternary **2022**, *5*, 24. <https://doi.org/10.3390/quat5020024>

Academic Editors: Philip Hughes and Susan Ivy-Ochs

Received: 20 October 2021

Accepted: 16 February 2022

Published: 16 April 2022

Publisher's Note: MDPI stays neutral with regard to jurisdictional claims in published maps and institutional affiliations.



Copyright: © 2022 by the authors. Licensee MDPI, Basel, Switzerland. This article is an open access article distributed under the terms and conditions of the Creative Commons Attribution (CC BY) license (<https://creativecommons.org/licenses/by/4.0/>).

1. Introduction

Caves are considered valuable paleogeographic [1] and paleoclimatic archives [2,3]. They are shaped by karstification resulting from underground flowing water and are influenced by tectonic activity, as well as regional and global climate change, thus recording the evolution of the surficial environment [1]. The imprints of these processes can be traced to contribute to the reconstruction of the paleogeography of an area by interpreting the preserved landforms. Sometimes the only remaining features can be found in caves, as exogenic processes entirely erase such data. Paleoclimatic studies in caves take advantage of the climate encoded in speleothems [4–6], but limited attention has been given, so far, to the potential of cave morphology and surrounding karst geomorphology in revealing encrypted paleoclimatic signals.

The expansion and retreat of Late Quaternary global ice masses directly influenced the global sea level [7], inducing the latter in a 125 m fluctuating range. The landscape

evolution triggered by these changes can be reconstructed from exogenic landforms, as well as the underground settings of coastal caves.

The peri-Mediterranean region hosts a large part of the world's coastal karst. Numerous studies focusing on paleoclimate [8–11], as well as sea-level changes [12–15], have taken advantage of this unique setting and shed light on the Mediterranean configuration during the Late Pleistocene and Holocene periods. Such studies use carbonate sea-level markers (speleothems, phreatic overgrowths on speleothems (POS), tidal notches, and marine terraces) in order to reconstruct the evolution of coastal Mediterranean paleogeography.

Besides these landforms, the integration of other cave features (e.g., cave deposits) may also help to identify the paleohydrological regime shifts a karstic system has undergone through time. For instance, the importance of deposits and their successions found in caves has not been adequately taken into account [16], particularly when combined with other sea-level indicators in coastal cave systems, such as marine terraces and tidal notches.

Selinitza Cave (SW Peloponnese, Greece) comprises a coastal cave, with the largest part situated above the present sea level, owing to the active tectonic regime of the area. Certain morphological features of the cave environment indicate the previous successive positions of the cave in the phreatic and epiphreatic zones. The objective of the present study is to present hypotheses concerning the paleogeographic evolution of Selinitza Cave, as well as its hydrologic changes, during the Quaternary. This study employs a combination of 3D cave mapping and a survey of geomorphological and biological indicators, as well as the texture, mineralogy, and trace element geochemistry of cave deposits. The results of this study are contextualized within a suggested climate regime and in extension to certain paleoclimatic periods during which coastal caves recorded past high sea-level stands, particularly in Greece.

2. Geotectonic Context

Selinitza Cave (36°48'10.48" B, 22°17'51.37" E, floor entrance at 18 m above sea level; henceforth asl) is located 46 km south of Kalamata City on the western flank of Taygetos Mountain (Figure 1). It is part of a 3.5 km composite karst system located on the western shores of Messiniakos Gulf, comprising Selinitza and Drakos underground river caves [17]. Messiniakos Gulf is a NNW-SSE asymmetric graben of the Late Miocene age [18] formed as a result of active tectonic processes in the western Hellenic Arc, an area with an intense geodynamic regime, i.e., seismicity, normal faulting, and crustal uplift [19]. It borders the Mani Peninsula to the west and is 50 to 80 km east of the Hellenic subduction zone. Neotectonic activity is prominent along the NNW-SSE-oriented faults and, to a lesser extent, along the E-W-oriented faults [20].

Selinitza Cave and its surroundings have been strongly influenced by both regional and local tectonic activity affecting the geomorphological evolution of Mani Peninsula. The lithology of the studied region comprises the Plattenkalk unit (PLK), mainly composed of pelagic, medium-to-thin-bedded, semi-crystalline, Late Senonian–Late Eocene gray to whitish limestones [21] corresponding to the deepest structural (autochthonous) unit of the Peloponnese [22,23]. The cave developed exclusively in the aforementioned lithology. In the surrounding area, there are also outcrops of flysch and Vigla limestones of the PLK unit (Figure 1). The interplay between tectonic and climatic conditions throughout Quaternary has left its imprint on the well-preserved marine terraces in the wider area.

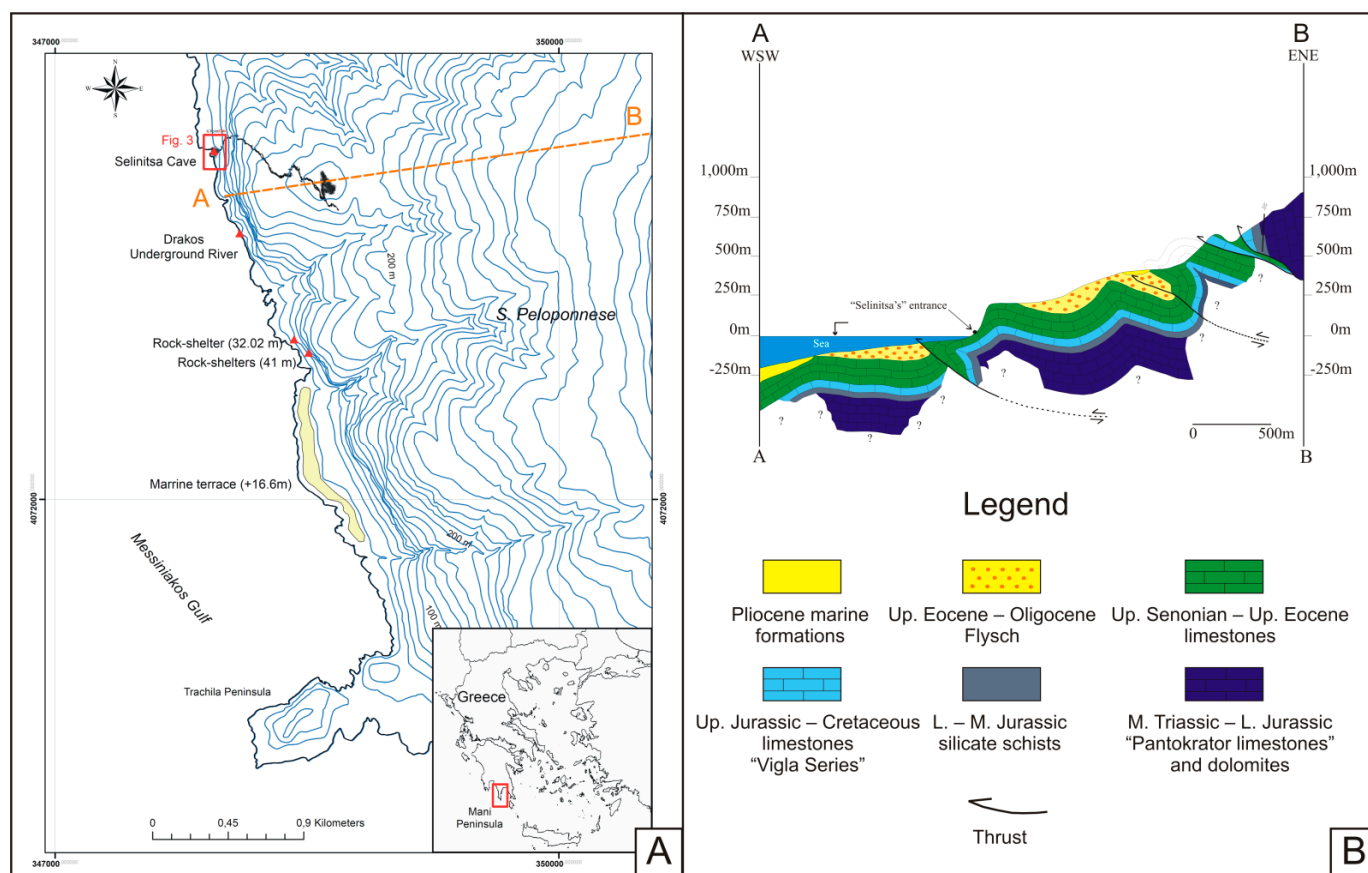


Figure 1. (A). Map of the studied area in SW Peloponnese. Blue contour lines represent surficial topography. Red triangles depict the location of geomorphological landforms discussed in the text, and the yellow area represent the surficial extent of the marine terrace at 16.6 m asl. (B). Geological depiction of the entrance and host lithologies of Selinitza Cave.

3. Materials and Methods

We performed a 3D laser mapping of Selinitza Cave, as well as the tidal notches across the entrance and the cave deposits inside the cave, in order to document its geomorphology. The 3D point cloud comprises 385 million points and exhibits speleomorphology with an accuracy of 2–3 cm. Laser mapping was conducted with a GeoSLAM ZEB-REVO portable laser scanner with simultaneous localization and mapping (SLAM) technology. The uncertainty of elevation measurements is ± 0.03 m. The 3D data were assessed using CloudCompare version 2.10.2. The 3D point cloud of the cave, as well as its peculiar geomorphological and biological landforms, were georeferenced with a Javad Triumph-2 real-time kinematic global navigation satellite system (RTK-GNSS) based on five fixed geographical points measured in the outer environment. The elevation of all geomorphological and biological landforms reported in this study was measured with the aforementioned RTK-GNSS device, with an accuracy of ± 0.03 m on both the horizontal and vertical axes. The precise morphology (profile) of the upper and lower notches was reconstructed by means of photogrammetry, allowing for the generation of two 3D models with Agisoft Photoscan software [24].

Moreover, in order to further define the prevailing paleohydrologic conditions within Selinitza Cave during its evolution, we also sampled infill identified during field work and mapping. These deposits include fine-grained material identified in a large chamber approximately 565 m from the entrance of the cave, as well as clogging material filling cracks, voids, joints, and faults in the same area (Figure 2). Samples of the fine-grained deposits were collected from several depths, whereas samples of the clogging material were

hand-picked from several locations in the same area. Mineralogy and texture of the collected samples was determined by combination of transmitted-light optical microscopy, X-ray diffraction (XRD), scanning electron microscopy (SEM), and Raman spectroscopy (details on the employed techniques are available in the Supplementary Materials). Besides textural and mineralogical analyses of the fine-grained deposits, we also performed geochemical analyses of the material in order to define its origin and correlate it with the paleogeographic evolution of the Selinitza Cave. The cave deposits were commercially analyzed for major and trace elements at ALS Laboratories (Ireland) (see Supplementary Material for details). Geochemical analyses and the calculated standard deviation (S.D.) for the whole suite of elements are presented in Table S1.

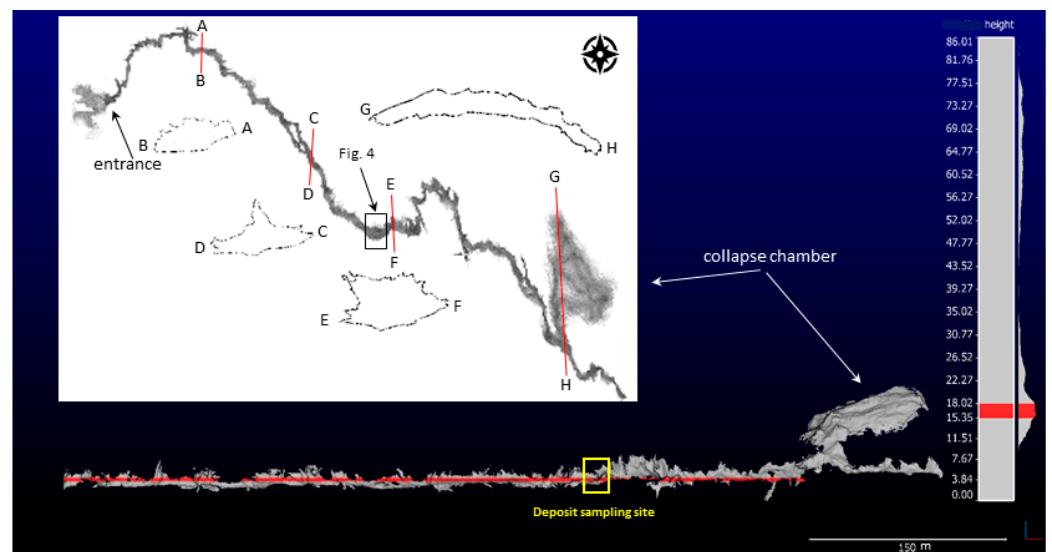


Figure 2. Side view of the 3D point cloud of Selinitza Cave, with the location of the fine-grained deposit indicated by a yellow square. The thick red line represents the largest space volume of the cave. The embedded figure is a top view of the 3D point cloud of the cave with the respective cross-sections labeled A to H. The height of 3D mapping is given in respect to the present sea level and its histogram.

4. Results

4.1. Three-Dimensional Mapping and Cave Morphology

The speleogenesis of the Selinitza cave system is determined by the main tectonic structures of the area. The main cave passage (Figure 2) follows the NW-SE Late Miocene tectonic discontinuities [17,25], whereas Drakos mainly follows the NE-SW Mid-Late Pleistocene tectonic direction. The entrance floor of Selinitza Cave lies at 18 m asl, whereas Drakos is located 10 m underwater and 500 m south of Selinitza [26]. Selinitza is mainly a dry cave, partially extending underwater. The cave system extends 80 m in depth, with a large underwater portion still unexplored. Thus, the karstification base of the cave system and, by extension, of the entire area, cannot be precisely determined.

3D mapping of Selinitza revealed the development of the cave passages following a general NW-SE direction, in agreement with [25] (Figure 2). The entrance of the cave is located 47.6 m from the coastline. The bedding plane at the entrance is horizontal, dipping to the WSW ($10^\circ/267^\circ$). The bedding plane changes direction to NE ($19^\circ/029^\circ$) 90 m from the entrance, implying a structural fold. The limestone bedding plane seems to play a secondary role in the speleogenetic process, as some passage segments follow the geometry of the bedding plane. The main corridor has a maximum elevation of ~ 32 m. The 'big hall', 8.5 m above the main conduit, represents a collapse chamber with an area of 252×154 m, featuring a triangular shape. A NW-SE fault ($81^\circ/250^\circ$) delimits the western side of this chamber, comprised of breakdown deposits and boulders larger than 1 m^3 . The bedding

plane at the chamber's roof ranges between $25^{\circ}/020^{\circ}$ and $30^{\circ}/050^{\circ}$. The altitudinal range of the cave is between 18 and 86 m. The collapse chamber extends from 40.58 to 86 m (Figure 2), and the epikarst zone above it reaches a width of 134 m. This chamber has no connection to the surface. The largest space volume in Selinita Cave is found between 15.73 and 18.05 m (thick red line, Figure 2). The peak of the latter range is 16.4 m.

4.2. Geomorphological and Biological Sea-Level (SL) Indicators

Fieldwork revealed geomorphological and biological SL indicators in the vicinity of the Selinita Cave entrance. Four marine terraces are present at 6 m, 10.7 m, 16.6 m, and 30–32 m asl between Selinita and Trachila Peninsula (Figure 1). The lower terrace at 6 m asl is mainly visible at Trachila, whereas the most prominent terrace in the region is 16.6 m asl. The terrace between 30 and 32 m asl is an almost flat surface above the entrance of Selinita, along which the main road is constructed (Figure 3). This shoreline/terrace at 30–32 m asl is also documented by the presence of a notch horizon at 32.02 m asl in a small shelter. The shelter opens ~10 m from the sea, approximately 1.2 km southeast of Selinita, and faces seawards; this could be a flank margin cave. Two other tidal notches are present: one below the cave entrance at +15.32 m asl and the second above the cave entrance at +16.4 m asl (Figure 3).

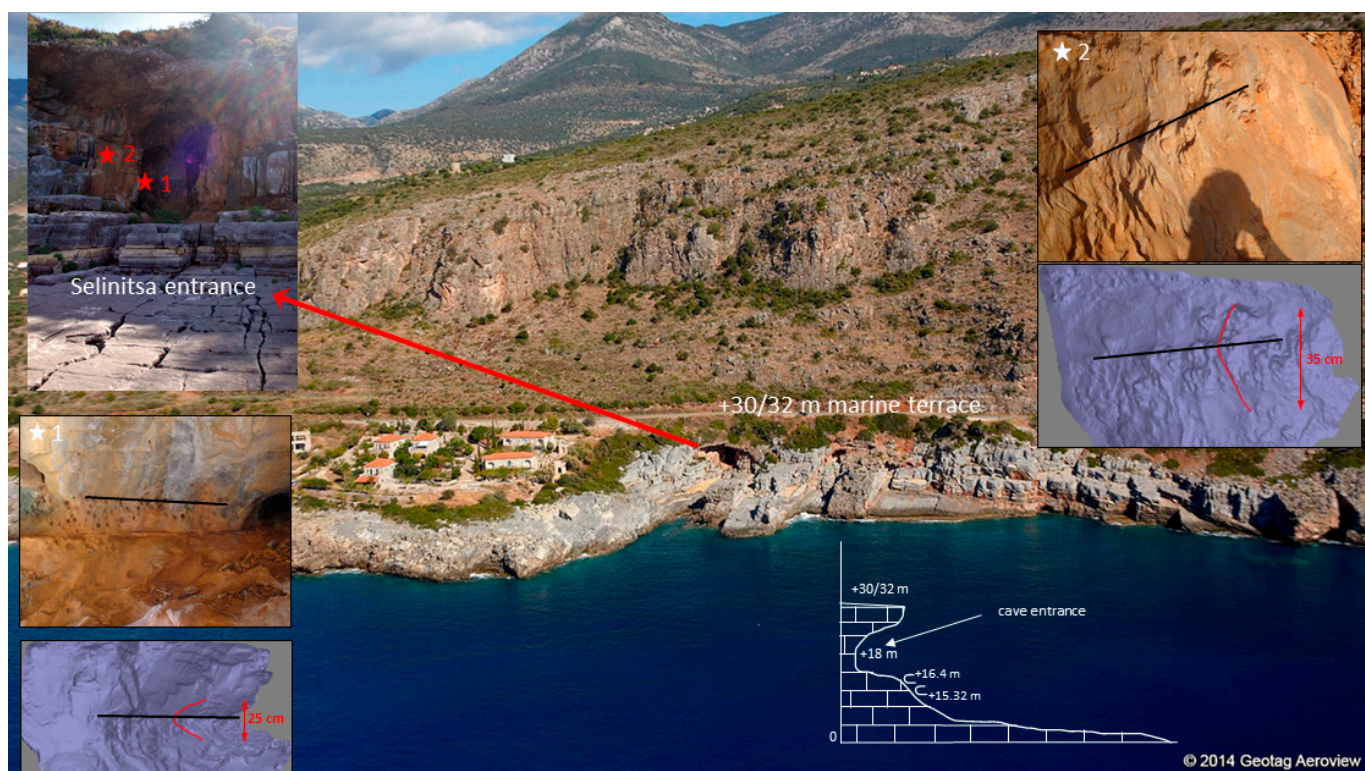


Figure 3. View from the west of the entrance to Selinita Cave and its wider coastal area. The embedded pictures (1 and 2) show the lower and upper notch (*1 and *2, respectively), as well as their 3D models, respectively. The black lines in the images depict former mean sea levels. The schematic section on the bottom right addresses the vertical arrangement of the area's geomorphological features.

The biological sea-level indicator used in this study is the numerous *Lithophaga* borings that occur between the present sea level and 45 m asl. These borings are hollows in limestone created by endolithic *Lithophaga* bivalves that live in the upper 30 m of the water column [27,28]. The highest frequency of *Lithophaga* populations usually coincides with the first few meters below sea level, with their upper limit at the mean sea level [29]. Consequently, when these mollusk burrows are well delineated and/or are correlated

with another morphological indicator, such as a tidal notch, they constitute a biological sea-level proxy [27]. In this case, attention should be given to populations with a horizontal clearcut upper limit. The upper limit of *Lithophaga* boreholes has been used to date RSL changes [30–32] or as a sea-level indicator in submerged speleothems [33]. Other geomorphological landforms include two small caves and a partially preserved coastline located at ~41 m asl with *Lithophaga* biological perforations in a horizontal configuration.

4.3. Fine-Grained Cave Deposits, Clogging Material

The Selinitza cave deposits show consistent mineralogy, geochemistry, and texture from top to bottom (Figure 4). The material is fine-grained, unsorted, and predominated by angular–subangular quartz fragments (detritus) and euhedral to subhedral dolomite crystals, which are occasionally pitted (Figures 4, 5, S2 and S3). Muscovite laths, albite, anorthite, angular to subangular calcite, Mg-calcite, and Fe-oxides/hydroxides are less abundant (Figures S4–S7), the latter providing reddish color to the deposits. Moreover, traces of apatite, rutile, sphene, and barite are also present (Table 1). The clogging material filling cracks, voids, and faults in Selinitza Cave is predominated by quartz, with minor chlorite and muscovite, whereas no carbonates were identified (Table 1, Figure S1).

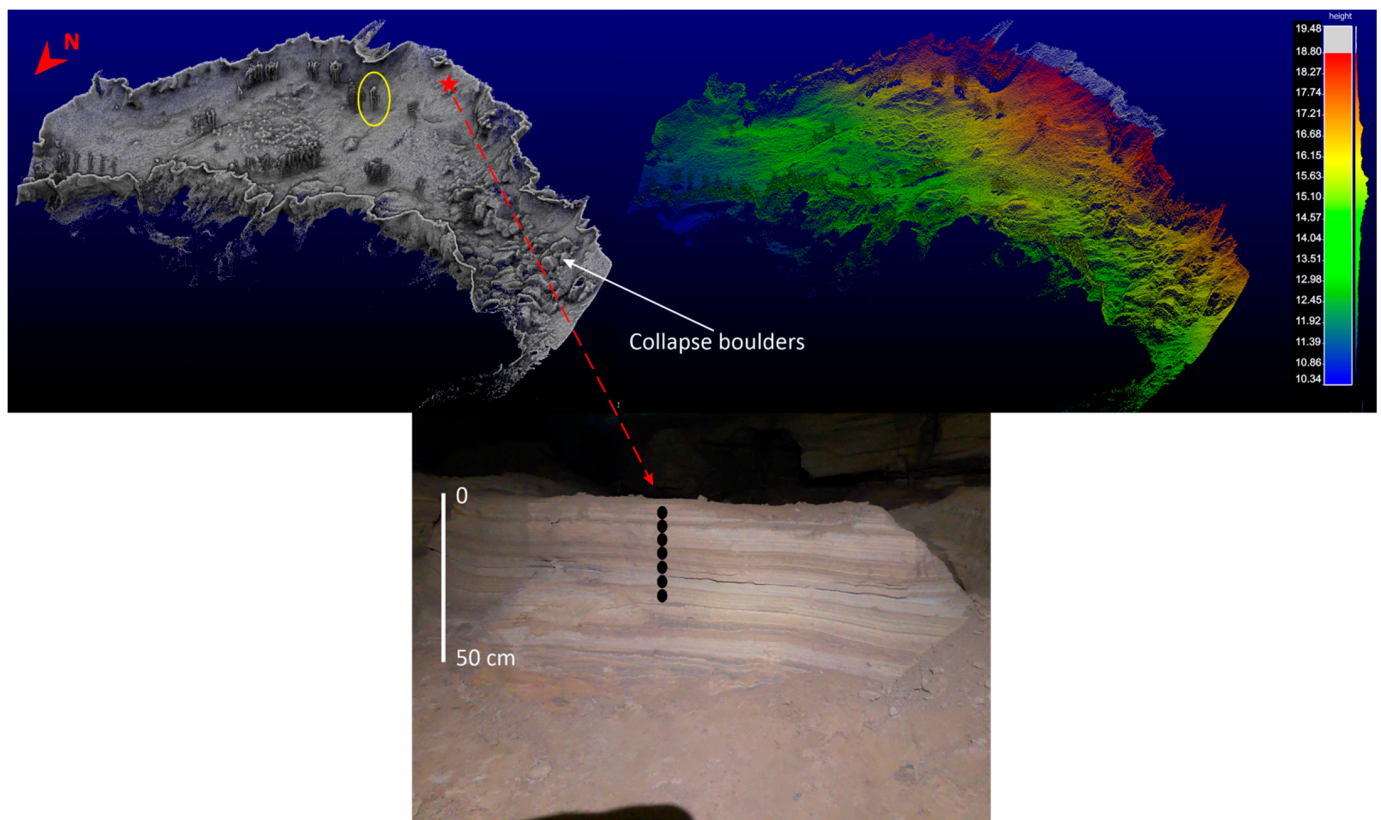


Figure 4. View of the chamber where the fine-grained cave deposits were sampled (upper images, after 3D mapping). The red star depicts the exact deposit site. View of the passage with its height distribution in a color scale (upper right image). The fine-grained deposits and corresponding sampling points are depicted with black circles (bottom image). The yellow ellipse indicates the figure of the researcher operating the 3D scanner.

The cave deposits sampled at 565 m from the entrance show Si content ranging from 57.4 to 62.2 (as SiO_2 wt%) and Al and Fe content ranging from 6.03 to 7.69 and 2.33 to 2.71 (as Al_2O_3 wt% and Fe_2O_3 wt%), respectively. Ca content is high, largely attributed to the presence of carbonates, primarily dolomite and, to a lesser extent, calcite and Mg-calcite (7.02 to 9.61 as CaO wt%), whereas Mn, K, and P contents are lower (Table S1). Mg content

ranges between 4.93 and 6.17 (as MgO wt%) and is closely related to the abundance of dolomite in the sediment material. Sr content in the cave sediment is low (ranging between 55.9 and 67.3 ppm), whereas total REE values (Σ REE) are between 105.79 and 125.16 ppm, with higher values for LREEs (91.99 to 109.53 ppm) relative to HREEs (13.80 to 15.38 ppm) (Table S1).

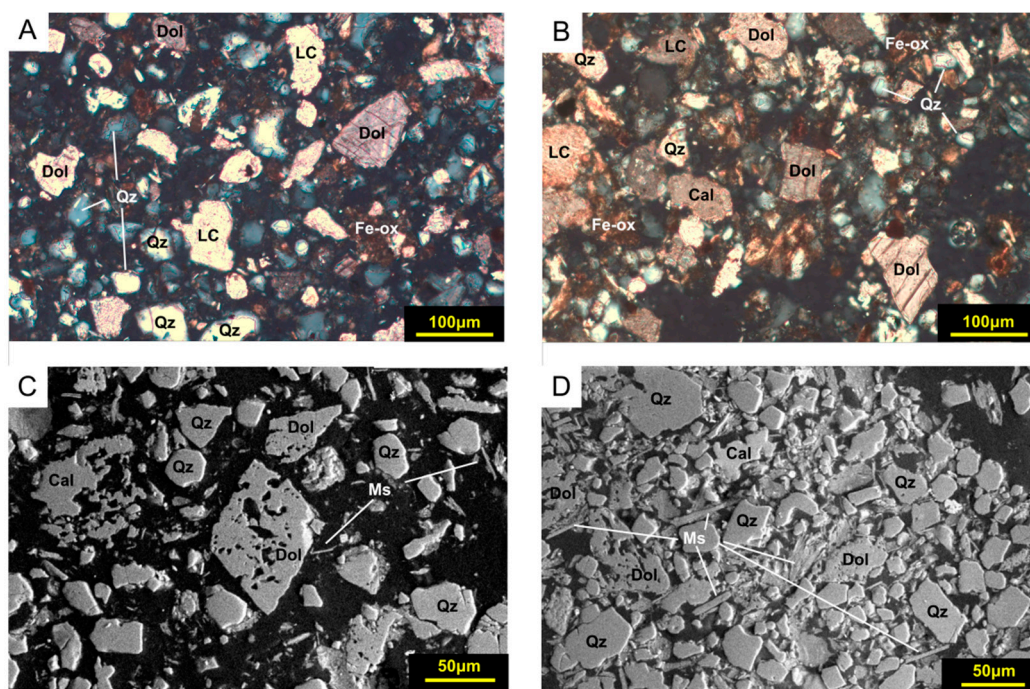


Figure 5. (A,B) Transmitted-light, crossed-polarized, thin-section photomicrographs of fine-grained deposits from Selinitza Cave. Detrital, angular–subangular quartz clasts (Qz) and euhedral to subhedral authigenic dolomite (Dol) predominate, whereas small lithic clasts (LC) are also observed. (C) Back-scattered electron microphotograph of Selinitza fine-grained deposits. The presence of euhedral to subhedral authigenic dolomite (dol) and detrital, angular quartz fragments (Qz) is evident. Minor muscovite clasts (Ms) are also present, along with traces of anhedral calcite (Cal). (D) Back-scattered electron microphotograph of a lithic clast (LC) from Selinitza fine-grained deposits with predominating angular to subangular quartz (Qz) clasts, minor muscovite laths (Ms), and traces of anhedral calcite. Mineral abbreviations taken from [34].

Table 1. Semi-quantitative mineralogical analyses of the different deposit facies in Selinitza Cave identified by optical microscopy, X-ray diffraction, Raman spectroscopy, and scanning electron microscopy.

Facies/Mineral	Qz	Dol	Ms	Cal (sp)	Chl	Hem/Gth	An	Ab	Ap	Rt	Zrn
Fine-grained deposits	+++++	+++++	+++	+	+	+	+	+	+	+	+
Clogging material	+++++		+++		+++						

+++++ major phase, +++ minor phase, + traces. Mineral abbreviations taken from [34]; Qz: quartz; Dol: dolomite; Ms: muscovite; Cal (sp): calcite species, including calcite and Mg-calcite; Chl: chlorite; Hem: hematite; Gth: goethite; An: anorthite; Ab: albite; Ap: apatite; Rt: rutile; Zrn: zircon.

5. Discussion

Although Selinitza Cave is located on the shore, it shows evidence of phreatic/epiphreatic origin (tubular galleries, upstream divergence of passages, and scallops). The cave was once flooded, as Drakos is now, and due to tectonic uplift affecting the area, the cave passages are now in the vadose zone. On the contrary, the overall morphology of Drakos lies underwater and comprises successive karstified base levels [25] most likely corresponding to sea-level stands postdating the Last Glacial Maximum (LGM).

The vertical movement of the land relative to the sea is also evidenced by geomorphological sea-level markers, including tidal notches. The latter accurately depict former sea-level stands, formed as a result of bioerosion processes in the intertidal zone [35]. The presence of tidal notches in uplifting coastlines is indicative of the vertical motion of the land. At Selinitsa Cave, the lower notch at 15.32 ± 0.03 m asl has a symmetric profile, with a height of 25 ± 0.03 cm, whereas the upper notch (height $\sim 35 \pm 0.03$ cm) has a more open profile (Figure 3). Both notches correlate well with a horizontal arrangement of *Lithophaga* borings, with higher perforation frequency at the maximum retreating point of the notches (vertex). Consequently, the notches and *Lithophaga* borings represent former sea-level stands. Furthermore, 3D scanning data provide evidence concerning the altitudinal range of intense karstification. The highest volume of the cave ranges between 15.73 and 18.05 m asl (thick red line, Figure 2), representing the space where the major karstification phase of Selinitsa's development took place. It also correlates well with the geomorphological features of the area, such as the upper notch (16.4 m) at the cave entrance (Figures 3 and 6) and the marine terrace at 16.6 m. The peak of this karstification range lies at 16.4 m asl and represents the level where the phreatic/epiphreatic zone was stable for a sufficient period of time, resulting in the widening of the cave passage (Figures 2 and 6). Additionally, the marine terrace at 16.6 m supports the hypothesis that the sea stood at the level of the widest space resulting from the chemical dissolution of the host carbonate rocks (Upper Senonian–Upper Eocene limestones, Figures 1B and 2). Similar morphological features (widened passages) indicating successive sea-level positions can also be seen in the submerged cave of Drakos to the south [25].

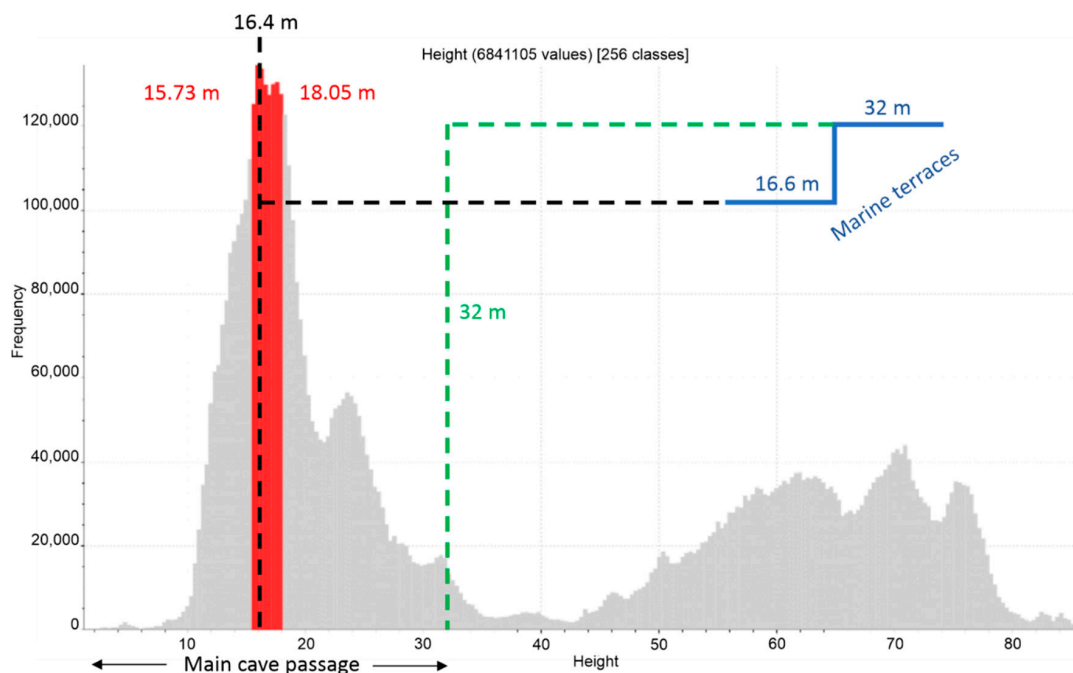


Figure 6. Histogram of the height frequency of Selinitsa Cave, extracted by 3D scanning. The horizontal axis corresponds to the height, and the vertical axis corresponds to frequency. The red range depicts the largest space in the cave. The black dotted line shows the peak of the latter space, whereas the green dotted line delimits the height of 32 m. Both heights are correlated with the marine terraces of the studied area.

Moreover, the maximum elevation of the main passage of Selinitsa Cave at 32 m provides additional evidence of the phreatic/epiphreatic functioning of the cave when correlated to the tidal notch with a *Lithophaga* horizontal arrangement at 32.02 m (Figures 3 and 6). This notch constitutes a biological sea-level proxy and pinpoint to a sea-level stand

at this elevation. The divergence and tubular cross-sectional shape of the cave corridors, as well as the presence of scallops on the walls, can be explained by a past sea level at 32.02 m.

Other evidence of partial submergence in the phreatic/epiphreatic zone includes the presence of successive layers of fine-grained deposits (silt–clay alternations) in the inner part of the cave, about 565 m from the entrance to the far end [36]. In most karstic systems containing clastic deposits [16,37], a fine-grained, thin layer is deposited every time the cave is filled with water, and such deposits are characterized as “slack-water facies” [38]. These facies are usually observed at the uppermost part of a sedimentary succession [37], with low thickness, indicating a gradual decrease in the flowing speed of water. In the case of Selinitza Cave, field observations revealed increased thickness of the fine-grained sediment, exceeding 2 m in height (Figures 2 and 4). The morphology of Selinitza’s main conduit played a determinant role in the deposition of fine-grained material, particularly during periods when the sea level stood at higher elevations than at present. 3D mapping revealed that the cave becomes progressively tighter towards the entrance, with the narrowest passage ~55 m from the entrance. During periods of higher sea levels and conditions of increased water discharge by the cave system, water was unable to be successfully drained due to the aforementioned narrowing, which caused back flooding of the cave. A few meters beyond the fine-grained deposits, roof collapse led to the accumulation of sizeable limestone boulders (~1 m³), which significantly reduced the cave volume (Figure 4). Collapse material is present only in this part of the cave, and these collapses probably contributed to back flooding, as documented in other locations [16]. This observation, combined with the maximum altitude of the fine-grained deposits at 18.8 m asl, clearly indicates that for prolonged periods, this part of the cave was flooded by water forming stagnant ponds and small lakes, with the water level higher than sea level. The maximum elevation of the cave deposits is higher than all markers depicting former sea-level stands (notches and marine terraces). The adjacent markers at 15.32 m, 16.4 m, and 16.6 m asl support the hypothesis of a back flooding higher than sea level. Consequently, the fine-grained material was deposited on the pond floor, as had enough time to settle. The presence of clogging material in cracks, faults, and joints in the same area of the cave further contributed to the formation of these ponds. Presently, there are no active streams or pools in Selinitza; therefore, the fine-grained deposits indicate former phreatic/epiphreatic conditions that might have triggered back flooding of the upstream passages, especially in areas where clogging material is found (Table 1). As water recessed, deposition occurred along the main cave passage in areas where water was ponding. Similar sedimentary features have been reported and interpreted as the result of back flooding due to downstream cave-roof-collapse breccia in the Veľký Dóm segment of the Demänová cave system in Slovakia [16].

The textural features of the fine-grained deposits (unsorted, angular–subangular fragments) clearly point to small-scale, terrestrial transportation, rejecting possible penetration of detritus by sea-water flooding (Figure 5) and supporting the proposed explanation of back flooding. The trace element geochemistry of the fine-grained sediment suggests a continental source of detritus, pointing to the overlying Plattenkalk flysch (Figure 7).

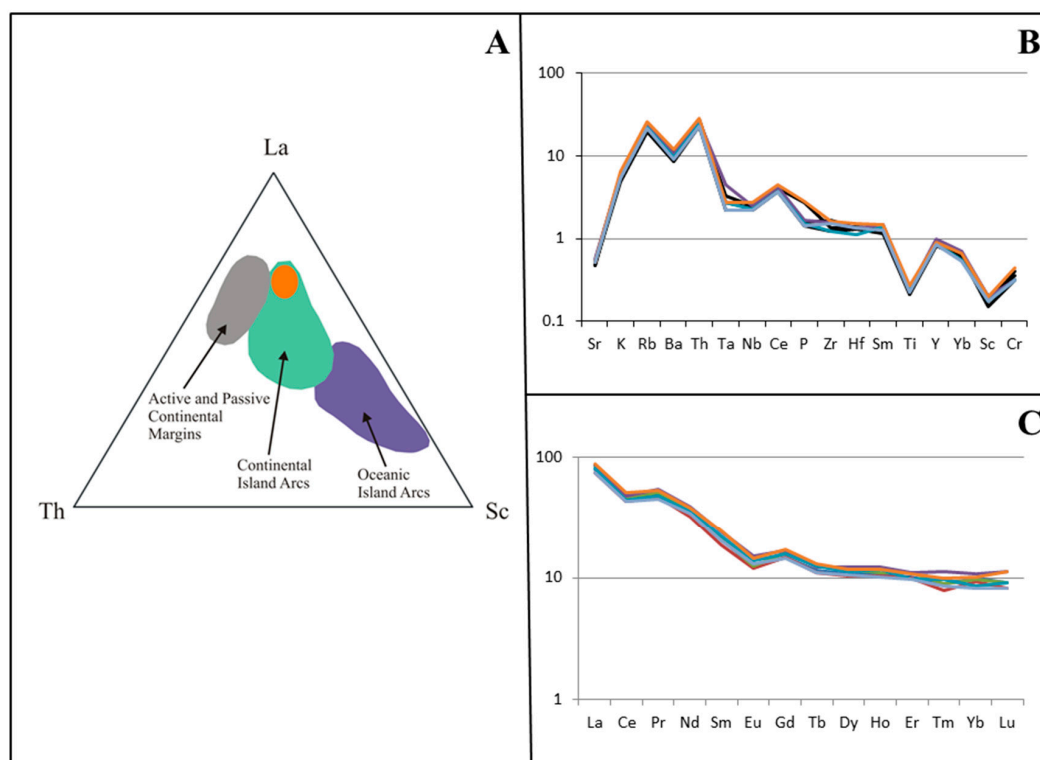


Figure 7. (A) Trace element La-Sc-Th ternary plot for Selinitza Cave fine-grained deposits (orange ellipse) (based on [39]). (B,C) Multi-element spider plots for Selinitza Cave fine-grained deposits. (B) MORB-normalized diagram (normalized values based on [40]). (C) REE-normalized diagram (normalized values based on [41]).

The predominance of dolomite in the cave sediment relative to calcite and Mg-calcite in the carbonate fraction (>98% modal), combined with the development of Selinitza in Upper Senonian to Upper Eocene limestones (Figure 1B), indicates that dolomite is authigenic and formed during settling of water in the cave ponds. Dolomite formation is favored in hyposaline environments (such as the Selinitza cave system) [42] following mixing of seawater and percolating fresh water. The texture of dolomite crystals found in the cave sediment (euhedral, romb-shaped, Figure 5) supports the authigenic character of dolomite. It is not clear whether dolomite originates from aragonite and/or calcite replacement, although the absence of CaCO_3 polymorphs in the cave sediment (<1% modal) supports the direct precipitation of dolomite in the cave ponds contemporaneously with sediment (penecontemporaneous or syndepositional according to the terminology of [42]). The presence of authigenic dolomite in sediments of Selinitza Cave indicates that for prolonged periods, dissolved Mg concentrations in the pond water remained both stable and high enough to favor its precipitation over calcite and/or aragonite, as in similar pCO_2 conditions, higher Mg activity leads to dolomite precipitation [43]. Higher Mg activity may also point to higher residence time of percolating (meteoric) water interacting with host lithologies (Figure 1B), thus increasing the dissolved Mg content of the settling water, eventually leading to primarily dolomite formation. Moreover, the predominance of dolomite through the entire sedimentary succession indicates a constant source of Mg in water in Selinitza Cave, either as a result of mixing fresh water and seawater, dissolution of host lithologies, or both in a stable geochemical environment for long periods of time.

With the aim of constraining a chronological framework for these processes, we used the available data from Diros Cave, located approximately 20 km south of Selinitza. In the area of Diros, geo-bio SL indicators occur in the range of 12–15 and 5–6 m asl, and according to [44], they are considered representative of MIS 5e and 5a sea-level stands, respectively. In the case of Selinitza Cave, we interpreted the marine terrace at 16.6 m as

an outcome of coastal erosion during MIS 5. Although the values are slightly dissimilar between the two caves, the discrepancy may be attributed to different uplift rates of the Mani Peninsula. Kleman et al. [45] attributed the observed dissimilarity in this area to an upward tilting of the Mani pediment (the latter being of pre-Middle Pleistocene age, e.g., [46]) to the north, whereas Kelletat et al. [47] interpreted the altitudinal decrease in the MIS 5 terraces as a southward tilting of the entire western coast of the Mani Peninsula. Based on the aforementioned hypothesis, the two independent sources of sea-level data (peak volume at 16.4 m derived from 3D scanning and the marine terrace at 16.6 m asl) validate the presence of a Late Quaternary sea-level stand in the surficial area, as well as in the cave environment. The fine-grained deposits indicate that during this period, cave flooding took place, with the water column preserved at a higher level relative to the MIS 5 sea stand.

In conclusion, the multidisciplinary approach of the present study highlights the significance of 3D mapping and the implementation of geo-bio-SL indicators and sedimentology to decipher the paleogeographic evolution of coastal caves. The formation and evolution of Selinitsa Cave make it ideal for identifying the paleoclimate regime of Greece and eastern Mediterranean regions, as its development was largely affected by sea-level changes during the Late Quaternary. Combined with radiochronological data, the aforementioned may also reveal crucial information that could help constrain the time frame of Late Quaternary paleoclimatic regimes and the corresponding sea-level fluctuations in eastern Mediterranean regions.

6. Conclusions

The outcome of this study regarding the evolution of Selinitsa Cave during the Quaternary may be summarized as follows:

- In the area of Selinitsa Cave, there are four distinct marine terraces at 6, 10.7, 16.6, and 30–32 m asl, with the terrace at 16.6 m representing the MIS5 sea-level stand;
- 3D mapping revealed that the major volume of the cave clusters at 16.4 m asl, indicating that karstification occurred along the phreatic/epiphreatic zone, at approximately the same level as the MIS 5 marine terrace at 16.6 m asl;
- The fine-grained deposits found in the cave indicate cave flooding during MIS 5, and the increased sediment thickness suggests stable hydrologic conditions for prolonged time-periods (reduced speed of water flow), favoring deposition of fine-grained material;
- The detrital component of the deposits suggests a continental source based on major and trace element geochemistry (Plattenkalk flysch);
- The predominance of authigenic dolomite in the cave deposits indicates that the material was deposited in a setting where mixing of seawater with percolating water occurred and at a higher altitude relative to sea level;
- The geochemical and hydrologic regime of the settling ponds remained stable for prolonged time-periods, as authigenic dolomite occurs through the whole sedimentary succession;
- The multidisciplinary approach of this study may provide crucial information regarding the paleogeographic evolution of karstic systems, and such data may be employed to unravel the paleoclimate regime of the coastal zone of the eastern Mediterranean during the Late Quaternary.

Supplementary Materials: The following are available online at <https://www.mdpi.com/article/10.3390/quat5020024/s1>. Figure S1: Representative XRD pattern of the clogging material filling cracks, joints, voids and faults in Selinitsa Cave; Figure S2: Representative XRD pattern of the fine-grained deposits found in Selinitsa Cave; Figure S3: Representative XRD pattern of the fine-grained deposits found in Selinitsa Cave; Figure S4: Representative SEM-EDS spectrum of detrital albite from the fine-grained deposits from Selinitsa Cave; Figure S5: Representative SEM-EDS spectra of authigenic dolomite from the fine-grained deposits from Selinitsa Cave; Figure S6: Representative SEM-EDS spectrum of detrital muscovite from the fine-grained deposits from Selinitsa Cave; Figure S7:

Representative SEM-EDS spectrum of Mg-calcite from the fine-grained deposits from Selinita Cave; Table S1: Representative major (wt.%) and trace (ppm) element analyses of the fine-grained deposits in Selinita Cave.

Author Contributions: Conceptualization, I.K.; methodology I.K., S.T. and V.S.; software I.K.; investigation, I.K., S.T., V.S. and E.K.; writing—original draft preparation, I.K. and S.T.; writing—review and editing, I.K., S.T. and E.K. All authors have read and agreed to the published version of the manuscript.

Funding: This research is co-financed by Greece and the European Union (European Social Fund—ESF) through the Operational Programme «Human Resources Development, Education and Lifelong Learning 2014–2020» in the context of the project “Geochemical, mineralogical and petrographical investigation of crystalline carbonate deposits and speleothems of southwest Peloponnese and applications in paleo-environmental studies” (MIS 5049093).

Acknowledgments: The authors gratefully thank anonymous reviewers for their valuable comments and suggestions regarding the overall quality and presentation of the manuscript. The authors also wish to thank to Yiannis Psaltakis for his help during the 3D mapping of Selinita, as well as Landmark SA for use of the RTK-GNSS device.

Conflicts of Interest: The authors declare no conflict of interest.

References

1. Delannoy, J.-J.; Gauchon, C.; Hobléa, F.; Jaillet, S.; Maire, R.; Perrette, Y.; Perroux, A.-S.; Ployon, E.; Vanara, N. Karst: From palaeogeographic archives to environmental indicators. *Geomorphologie* **2009**, *15*, 83–94. [[CrossRef](#)]
2. McDermott, F. Palaeo-Climature Reconstruction from Stable Isotope Variations in Speleothems: A Review. *Quat. Sci. Rev.* **2004**, *23*, 901–918. [[CrossRef](#)]
3. Fairchild, I.J.; Baker, A. *Speleothem Science: From Process to Past Environments*; Wiley: Hoboken, NJ, USA, 2012.
4. Dorale, J.A.; Edwards, R.L.; Onac, B.P. Stable Isotopes as Environmental Indicators in Speleothems. In *Karst Processes and Carbon Cycle*; Daoxian, Y., Cheng, Z., Eds.; Geological Publishing House: Beijing, China, 2002; pp. 107–120.
5. Lachniet, M.S. Climatic and Environmental Controls on Speleothem Oxygen-Isotope Values. *Quat. Sci. Rev.* **2009**, *28*, 412–432. [[CrossRef](#)]
6. Frisia, S. Microstratigraphic Logging of Calcite Fabrics in Speleothems as Tool for Palaeoclimate Studies. *Int. J. Speleol.* **2015**, *44*, 1.
7. Rovere, A.; Stocchi, P.; Vacchi, M. Eustatic and Relative Sea Level Changes. *Curr. Clim. Chang. Rep.* **2016**, *2*, 221–231. [[CrossRef](#)]
8. Dumitru, O.A.; Onac, B.P.; Polyak, V.J.; Wynn, J.G.; Asmerom, Y.; Fornós, J.J. Climate Variability in the Western Mediterranean between 121 and 67 Ka Derived from a Mallorcan Speleothem Record. *Palaeogeogr. Palaeoclimatol. Palaeoecol.* **2018**, *506*, 128–138. [[CrossRef](#)]
9. Nehme, C.; Verheyden, S.; Noble, S.R.; Farrant, A.R.; Sahy, D.; Hellstrom, J.; Delannoy, J.J.; Claeys, P. Reconstruction of MIS 5 Climate in the Central Levant Using a Stalagmite from Kanaan Cave, Lebanon. *Clim. Past* **2015**, *11*, 1785–1799. [[CrossRef](#)]
10. Ünal-İmer, E.; Shulmeister, J.; Zhao, J.-X.; Tonguç Uysal, I.; Feng, Y.-X.; Duc Nguyen, A.; Yüce, G. An 80 Kyr-Long Continuous Speleothem Record from Dim Cave, SW Turkey with Paleoclimatic Implications for the Eastern Mediterranean. *Sci. Rep.* **2015**, *5*, 13560. [[CrossRef](#)]
11. Columbu, A.; Chiarini, V.; Spötl, C.; Benazzi, S.; Hellstrom, J.; Cheng, H.; De Waele, J. Speleothem Record Attests to Stable Environmental Conditions during Neanderthal–Modern Human Turnover in Southern Italy. *Nat. Ecol. Evol.* **2020**, *4*, 1188–1195. [[CrossRef](#)]
12. Antonioli, A.; Belardinelli, M.E.; Bizzarri, A.; Vogt, K.S. Evidence of Instantaneous Dynamic Triggering during the Seismic Sequence of Year 2000 in South Iceland: Dynamic Triggering in Iceland in 2000. *J. Geophys. Res.* **2006**, *111*, B03302. [[CrossRef](#)]
13. Surić, M.; Juračić, M. Late Pleistocene—Holocene Environmental Changes—Records from Submerged Speleothems along the Eastern Adriatic Coast (Croatia). *Geol. Croat.* **2010**, *63*, 155–169. [[CrossRef](#)]
14. Evelpidou, N.; Kampilis, I.; Pirazzoli, P.A.; Vassilopoulos, A. Global Sea-Level Rise and the Disappearance of Tidal Notches. *Glob. Planet. Chang.* **2012**, *92–93*, 248–256. [[CrossRef](#)]
15. Polyak, V.J.; Onac, B.P.; Fornós, J.J.; Hay, C.; Asmerom, Y.; Dorale, J.A.; Ginés, J.; Tuccimei, P.; Ginés, A. A Highly Resolved Record of Relative Sea Level in the Western Mediterranean Sea during the Last Interglacial Period. *Nat. Geosci.* **2018**, *11*, 860–864. [[CrossRef](#)]
16. Bella, P.; Gradziński, M.; Hercman, H.; Leszczyński, S.; Nemeček, W. Sedimentary Anatomy and Hydrological Record of Relic Fluvial Deposits in a Karst Cave Conduit. *Sedimentology* **2021**, *68*, 425–448. [[CrossRef](#)]
17. Papadopoulou-Vrynioti, K.; Kampilis, I. Formation and Development of a Karstic System below and above Sea Level in Messinian Mani Peninsula (S. Greece). *Speleogenesis Evol. Karst Aquifers* **2012**, *12*, 17–21.
18. Pavalakis, P.; Papanikolaou, D.; Chronis, G.; Lykoussis, B.; Anagnostou, G. Geological Structure of Inner Messiniakos Gulf. Pdf. *Bull. Geol. Soc. Greece* **1989**, *3*, 333–347.

19. Fountoulis, I. Quaternary Basin Sedimentation and Geodynamics in SW Peloponnese (Greece) and Late Stage Uplift of Taygetos Mt. *Boll. Geofis. Teor. Appl.* **2014**, *55*, 303–324. [[CrossRef](#)]
20. Mariolakos, I.; Papanikolaou, D.; Lagios, E. A Neotectonic Geodynamic Model of Peloponnesus Based on: Morphotectonics, Repeated Gravity Measurements and Seismicity. *Geol. Jahrb.* **1985**, *50*, 3–17.
21. Institute of Geology and Mineral Exploration. *Geological Map of Greece-Xiropkampion Sheet*; Institute of Geology and Mineral Exploration: Athens, Greece, 1983.
22. Mountrakis, D. *Geology of Greece*, 1st ed.; University Studio Press: Thessaloniki, Greece, 1985.
23. Doutsos, T.; Koukouvelas, I.; Poulimenos, G.; Kokkalas, S.; Xypolias, P.; Skourlis, K. An Exhumation Model of the South Peloponnesus, Greece. *Int. J. Earth Sci.* **2000**, *89*, 350–365. [[CrossRef](#)]
24. De Melo e Silva, H.; Brooks, C.; Dobson, R.; Ebling, J.; Evans, D.; Hart, B.; Oats, R.; Roussi, C.; Vaghefi, K. *3D Photogrammetry*; Memo 11; MichiganTech Transportation Institute: Houghton, MI, USA, 2011; p. 15.
25. Papadopoulou-Vrynioti, K.; Kampilis, I. The “Selinita-Drakos” Coastal Karstic System in the Messinian Mani Peninsula (Southwestern Greece) in Relation to the Terrestrial Geoenvironment. *Geol. Balc.* **2011**, *40*, 75–83. [[CrossRef](#)]
26. Kampilis, I. Geomorphological Study of the Submarine Karstic System of Drakos Underground River, Messinian Mani. Bachelor’s Thesis, University of Athens, Athens, Greece, 2007.
27. Laborel, J.; Laborel-Deguen, F. Biological Indicators of Relative Sea-Level Variations and of Co- Seismic Displacements in the Mediterranean Region. *J. Coast. Res.* **1994**, *10*, 395–415.
28. Schneiderwind, S.; Boulton, S.J.; Papanikolaou, I.; Kázmér, M.; Reicherter, K. Numerical Modeling of Tidal Notch Sequences on Rocky Coasts of the Mediterranean Basin: Tidal Notch Modeling. *J. Geophys. Res. Earth Surf.* **2017**, *122*, 1154–1181. [[CrossRef](#)]
29. Rovere, A.; Antonioli, F.; Bianchi, C.N. Fixed Biological Indicators. In *Handbook of Sea-Level Research*; Shennan, I., Long, A.J., Horton, B.P., Eds.; John Wiley & Sons, Ltd.: Chichester, UK, 2015; pp. 268–280. [[CrossRef](#)]
30. Lambeck, K.; Anzidei, M.; Antonioli, F.; Benini, A.; Esposito, A. Sea Level in Roman Time in the Central Mediterranean and Implications for Recent Change. *Earth Planet. Sci. Lett.* **2004**, *224*, 563–575. [[CrossRef](#)]
31. Ferranti, L.; Antonioli, F.; Mauz, B.; Amorosi, A.; Dai Pra, G.; Mastronuzzi, G.; Monaco, C.; Orrù, P.; Pappalardo, M.; Radtke, U.; et al. Markers of the Last Interglacial Sea-Level High Stand along the Coast of Italy: Tectonic Implications. *Quat. Int.* **2006**, *145–146*, 30–54. [[CrossRef](#)]
32. Falkenroth, M.; Adolphs, S.; Cahnbley, M.; Bagci, H.; Kázmér, M.; Mechernich, S.; Hoffmann, G. Biological Indicators Reveal Small-Scale Sea-Level Variability During MIS 5e (Sur, Sultanate of Oman). *Open Quat.* **2020**, *6*, 1. [[CrossRef](#)]
33. Antonioli, F.; Oliverio, M. Holocene Sea-Level Rise Recorded by a Radiocarbon-Dated Mussel in a Submerged Speleothem beneath the Mediterranean Sea. *Quat. Res.* **1996**, *45*, 241–244. [[CrossRef](#)]
34. Whitney, D.L.; Evans, B.W. Abbreviations for Names of Rock-Forming Minerals. *Am. Mineral.* **2010**, *95*, 185–187. [[CrossRef](#)]
35. Pirazzoli, P.A. Marine Notches. In *Sea-Level Research: A Manual for the Collection and Evaluation of Data*; Van de Plassche, O., Ed.; Geo Books: Norwich, UK, 1986; pp. 361–400.
36. Kampilis, I.; Skliros, V.; Triantafyllidis, S. Quaternary Evolution and Paleoclimatology of the Coastal Cave of Selinita (SW Peloponnese, Greece) Based on Geomorphological and Geochemical Data. *EGU Gen. Assem. Conf. Abstr.* **2021**, EGU21-6516. [[CrossRef](#)]
37. White, W.B. Cave sediments and paleoclimate. *J. Cave Karst Stud.* **2007**, *69*, 76–93.
38. Bosch, R.F.; White, W.B. Lithofacies and transport of clastic sediments in karstic aquifers. In *Studies of Cave Sediments: Physical and Chemical Records of Paleoclimate*; Sasowsky, I.D., Mylroie, J., Eds.; Springer: Dordrecht, The Netherlands, 2007.
39. Bhatia, M.R.; Crook, K.A.W. Trace Element Characteristics of Graywackes and Tectonic Setting Discrimination of Sedimentary Basins. *Contr. Mineral. Petrol.* **1986**, *92*, 181–193. [[CrossRef](#)]
40. Pearce, J.A. Role of the Sub-Continental Lithosphere in Magma Genesis at Active Continental Margins. In *Continental Basalts and Mantle Xenoliths*; Hawkesworth, C.J., Norry, M.J., Eds.; Shiva Publishing: Nantwich, Cheshire, UK, 1983; pp. 230–249.
41. Nakamura, N. Determination of REE, Ba, Fe, Mg, Na and K in Carbonaceous and Ordinary Chondrites. *Geochim. Et Cosmochim. Acta* **1974**, *38*, 757–775. [[CrossRef](#)]
42. Machel, H.C. Dolomites. In *Encyclopedia of Geology*, 2nd ed.; Selley, R.C., Robin, I., Cocks, M., Plimer, I.R., Eds.; Elsevier: Amsterdam, The Netherlands, 2005; pp. 79–94.
43. Regattieri, E.; Zanchetta, G.; Drysdale, R.N.; Isola, I.; Hellstrom, J.C.; Dallai, L. Lateglacial to Holocene Trace Element Record (Ba, Mg, Sr) from Corchia Cave (Apuan Alps, Central Italy): Paleoenvironmental Implications: Trace Element Record from Corchia Cave, Central Italy. *J. Quat. Sci.* **2014**, *29*, 381–392. [[CrossRef](#)]
44. Bassiakos, I. Dating of Fossils from Caves and Speleothems: Evidence from Electron Spin Resonance (E.S.R.) Technique, the Study of Underground Karst Morphology and the Relevant Radiometric and Geological Conditions in Speleoenviroments of Dyros, Mani. (with English Abstract). Ph.D. Thesis, University of Athens, Athens, Greece, 1993.
45. Kleman, J.; Borgström, I.; Skelton, A.; Hall, A. Landscape Evolution and Landform Inheritance in Tectonically Active Regions: The Case of the Southwestern Peloponnese, Greece. *Z. Für Geomorphol.* **2016**, *60*, 171–193. [[CrossRef](#)]
46. Harvati, K.; Stringer, C.; Karkanias, P. Multivariate Analysis and Classification of the Apidima 2 Cranium from Mani, Southern Greece. *J. Hum. Evol.* **2011**, *60*, 246–250. [[CrossRef](#)]
47. Kelletat, D.; Kowalczyk, G.; Schroeder, B.; Winter, K.P. A Synoptic View on the Neotectonic Development of the Peloponnesian Coastal Regions: Zeitschrift Der Deutschen Geologischen Gesellschaft. *Z. Der Dtsch. Geol. Ges.* **1976**, *127*, 447–465.